Int. J. Nonlinear Anal. Appl.
Volume 12, Issue 1, Winter and Spring 2021, 59-74
ISSN: 2008-6822 (electronic)
http://dx.doi.org/10.22075/IJNAA.2021.4658

Linkage Factors Optimization of Multi-outputs of Compliant Mechanism using Response Surface

Rami Alfattani[a*], Mohammed Yunus[b], Turki Alamro[c], Ibrahim Alnaser[d]

[a,b,c,d] *Department of Mechanical Engineering, College of Engineering and Islamic Architecture, Umm Al-Qura University, Makkah, Kingdom of Saudi Arabia.*

Abstract

This paper presents a linkage factors synthesis and multi-level optimization technique for bi-stable compliant mechanism. The linkage synthesis problem is modeled as multiple level factors and responses optimization problem with constraints. The bi-stable compliant mechanism is modeled as a crank slider mechanism using pseudo-rigid-body model (PRBM). The model exerts the large deflection of flexible element which explains compliant mechanism's bi-stable performance. The design concept is applied on variable input parameters subsets. Though the effect of compliant mechanism process factors on F_{max} and PRBM deflection angle (Theta-cap Θ_1) are contradictory when studied individually as no response gives best process quality. The relationship model between input factors and responses characteristics were generated by ANOVA and optimized by response surface methodology (RSM). ANOVA shown more significant factors are the initial angle of link1 (θ_1) and material thickness (t). The Box-Behnken design of RSM is applied with a desirability function approach to determine the optimum set of parameters for minimizing F_{max} and maximizing the Theta-cap (Θ_1). Thus, this technique shown flexibility based on the product application could be tested and established.

Keywords: ANOVA, Compliant Mechanism, Particle Swarm Optimization, Linkage Design Factors, Surface Plots.

1. Introduction

This paper presents a design concept of bi-stable compliant mechanism and an optimization process based on selected output parameters. The design synthesis is pursued in step by step model that lead to final required parameters of the mechanism' dimensions. The bi-stable compliant mechanism

*Corresponding Author: Rami Alfattani
Email address: rafattni@uqu.edu.sa (Rami Alfattani[a*], Mohammed Yunus[b], Turki Alamro[c], Ibrahim Alnaser[d])

Received: February2020 *Revised:* October2020

is designed to act as deployable unit cell that require one degree of freedom (one actuation input). The deployable configuration occurs in many applications such as switches, gates, self-closing, and developable structures [1, 2]. These unit cells can be tessellated and arranged in organized pattern to perform shape-morphing systems [3, 4]. Moreover, many applications such airplane wings' flaps, deployable space antennas, and shape morphing structures benefit from the ability to morph the unit cell surface profile upon actuation [5-7]. If such designs have the ability to be manufactured at micro-scale, they could be used in applications as relays and medical grips [8, 9]. In automotive industry, Bistable compliant mechanism can be utilized in many applications including rear trunk lid of cars, and bumper collision absorber [9].

For this paper, the background is in the area of compliant mechanism and its modeling and design. A compliant mechanism obtains its mobility feature from flexible segment deflections hence eliminating the need for mechanical joints. Both performance and costs are influenced by reducing or eliminating mechanical joints. The mechanism has movable segments that are mostly thin than rigid. The thinner portions are often the first to deform when under displacement or when force is applied. There are two types of compliant mechanisms, which include partially and fully compliant mechanisms. There are no kinematic pairs in the mechanisms that are fully compliant. However, one or more joints like pins and sliders exist in partially complaint mechanisms. The benefit is reduced friction and wear reduced maintenance and weight, and higher reliability [1].

Besides, reducing assembly time affects costs because its design does not have hinges. Alteration of such a mechanism can be done by using a single piece hence reducing the number of parts. Precision in the compliant mechanism is increased because there are no friction forces caused by pin points hence lower vibrations [10, 11]. Therefore, compliant mechanisms are commonly used in instruments with high accuracy [12]. The type of mechanism is also used in commercial products such as compliant-based hinges. Moreover, with a compliant mechanism, a design can have the most effective way to attain robotic designs with mechanical stability [13]. There are challenges and limitations while using a compliant mechanism. One of these is stress relaxation or creep deformation if the compliant segment is subjected to an environment with excessive stress and temperature for long periods [14, 15]. Since movable segments are often used to store energy, it is challenging to stay within an elastic material range when the mechanism is deformed hence imposing limitations to the design[16]. So, researcher have developed approximation approaches to model compliant mechanisms.

Large-defection problems of compliant beams with loading condition are commonly solved using elliptic integral method [17, 18]; however, it difficult to drive closed-form solution for compliant mechanisms with loading conditions while approximation methods like Pseudo-Rigid-Body Models (PRBMs) is more useful particularly in designing compliant mechanisms [1, 19]. PRBMs is an approach that has been used to synthesize compliant mechanisms [1]. This research uses PRBMs to discuss further insight. Approaches that can be used as an alternative use strategy to achieve topology optimization and obtain a nonlinear compliant mechanism under particular input/output displacement [20]. Besides, Su applied the polynomial homotopy to create the four-bar compliant mechanism kinematic equations to solve particular design parameters [21]. Limaye used an approach that involves using a compliant mechanism kit that allows the formation of a designed mechanism and associates the characteristic from topology optimization [22].

The elements of bi-stable compliant mechanism were created using the PRBM approach, which was initially developed by Howell and Midha [1]. A comparison between the approximations and the Bernoulli-Euler beam equations were then made to derive a general approach to the PRBM approach and in accuracy quantification. The PRBM is a simpler approach used to evaluate and identify nonlinear beam behavior experiencing deflections. The approach makes approximations of the flexural beam by using torsional springs to combine two or more rigid links depending on the

beam's loading conditions. PRBM parameters include the torsional spring's location, the stiffness coefficient, and rigid link lengths. These parameters illustrate the nonlinear characteristic in the mechanical system's kinematic and force-deflection analysis. The compliant theory has been used to develop various types of PRBMs to produce the behavior of the flexural segment.

Soft computing methods have a wide range of applications [23-25]. Where more common theoretical approach for synthesis of compliant mechanism in terms of shape optimization or topology refers to Genetic Algorithm [26, 27], hybrid Taguchi-differential evolution algorithm [28], Gene Algorithm and Taguchi–based sensitivity analysis [29], and Response Surface Methodology (RSM) [30] and Particle swarm optimization. To simplify the design of CM using the kinematic dimension factors simultaneously, two stage approach namely, analyzing the link dimensions with PRB diagram and optimizing the dimensions of flexure hinges by RSM utilizing FEA results. Also, a multi-output optimization was applied to improve the static and dynamic characteristics of the linear compliant guide mechanism for high precision manufacturing processes. PRB diagram analysis by developing the kinematic relation of the links and a mathematical model was built by analytical method to improve the synthesis method of CM [paper]. Gradient-based optimization was employed to find the optimum link dimensions to reduce the number of design parameters. FEA results from ADPL codes in ANSYS of 3 D structural model is used in RSM with the help of assigned independent variables on outputs. The effect of these factors on responses were converted into the mathematical models to determine the optimum set of design variables.

One types of PRBM, the Fixed-Pinned cantilever beam that has a force at its end, will be used in this research. Flexural pivots that are small-length are used to model the Fixed-Pinned type of PRBMs using torsional springs. All other joints in CM are small-length flexural pivots that are large displacement hinges that have range of motion. Referring to extensive research work of previous researchers, it is noticed that, multi objective optimization of CM is necessary to understand the synthesis of CM. Work is divided into three stages, (1) for fixed pinned cantilever beam, important input and output variables are determined by PRBM. (2) Then using ANOVA, mathematical models based on higher order regression will be obtained and most influential factors will be notified. (3) Using Box-Behnken design of RSM is applied with a desirability function approach, a multi objective optimization will be performed to study different behaviors of the structure. Finally, optimum set of factors to meet minimum Fmax and maximum Theta-cap will be found out.

2. Design procedure

This section describes the model for a linear bi-stable compliant mechanism and the applied design procedures. The tool will rely on the crank-slider mechanism and consider large deflection analysis to illustrate the mechanism's bi-stable behavior. Derived from the Pseudo-Rigid-Body Model (PRBM), the kinetic and kinematic equations were numerically solved. The representation enables design of guideline generation. The parameters used in the design include the optimum anticipated deflection, widths of a compliant segment, selection of materials, optimal force needed to select actuator and optimal footmark such as the optimum rectangular area that fits the mechanism and in which the mechanism can freely move without any interference on other components.

The Pseudo-Rigid-Body Model (PRBM) is an essentially function strategy used in analyzing and synthesizing a bi-stable compliant mechanism. Howel and Midha first developed the approximations applied in the PRBM[31]. This approximation works by including the same behavior between rigid-body mechanism and compliant mechanisms. The model of link 1 of the bi-stable compliant mechanism is Fixed-Pinned PRBMs as indicated in Figure 1.

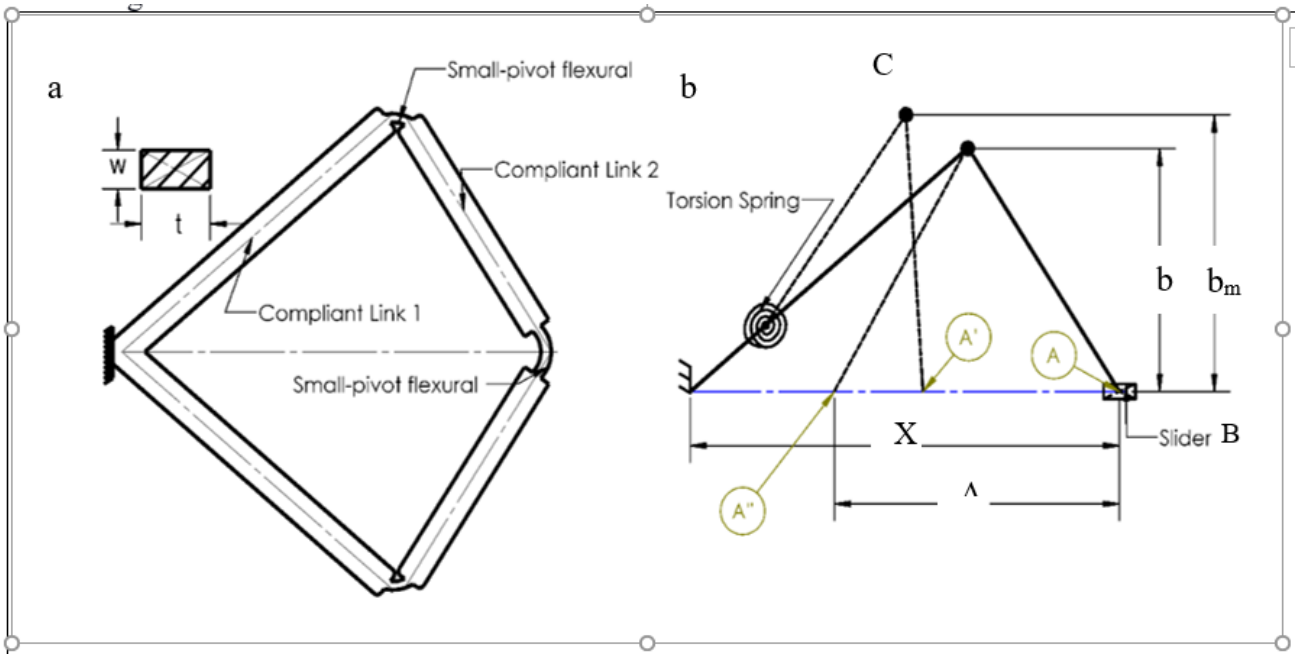

Figure 1: a) The bi-stable compliant mechanism. b) The PRBM replacement of the bi-stable compliant mechanism where A is the first stable configuration of the mechanism, A' is the unstable configuration, and A" is the second stable configuration.

To derive the force-displacement equation for the compliant mechanism, the method of virtual work was used as the standard method. At the same time, the constants provided by Howell were used as the PRBM constants, and they include the characteristic radius for the Fixed-Pinned γ, and stiffness coefficient $K\Theta$ as the table 1 [1].

Table 1: The constant coefficients for the Fixed-Pined PRBM adapted by [1]

	γ	K Θ
Fixed-Pined PRBM	0.85	2.65

The organization of this section will be divided into three essential parts. First, the theory underlies the bi-stable compliant mechanism model, and a description of how the model was derived from the PRBMs will be provided. Second, design approaches with dissimilar input will be illustrated using the step-by-step design. Thirdly, steps involved in deriving quadratic based regression models for the combination of inputs and outputs using ANOVA followed by RSM. Finally, steps for applying multi objective PSO based genetic algorithm with pareto front solver will be demonstrated.

2.1. Modeling of bi-stable compliant mechanism

The equations of the model were obtained by solving the kinetic and virtual work equations. Figure 2 show the notations, parameters, and sketch of the model. The compliant joints (B and C) are small-pivots flexural that obtain its motion feature by bending. The kinematic coefficient calculation used the kinematic equation. The kinematic coefficient was then replaced to form the virtual work equations. The equation of the model was numerically solved and plotted.

The mechanism gains its flexibility from link1 which experiences the large deflection. Link 2 will not deflect but it will transmit the force and displacement. Link 1 is spitted based on Pseudo-Rigid

Body model into two lengths l_1 and l_2 shown in Figure 2 (refer Eq. (1) and (2)).

$$L_1 = l_1 + l_2 \tag{1}$$
$$l_1 = (1-\gamma)L_1, l_2 = \gamma L_1 \tag{2}$$

The characteristic stiffness K_1 of the torsion spring at the Pseudo-Rigid-Body model of link 1 is (refer Eq. (3) and (4)) :

$$K_1 = \gamma K_\theta \frac{EI_1}{L_1}, I_1 = \frac{tw_1^3}{12} \tag{3}$$
$$K_2 = \gamma K_\theta \frac{2EI_2}{L_2}, I_2 = \frac{tw_1^3}{12} \tag{4}$$

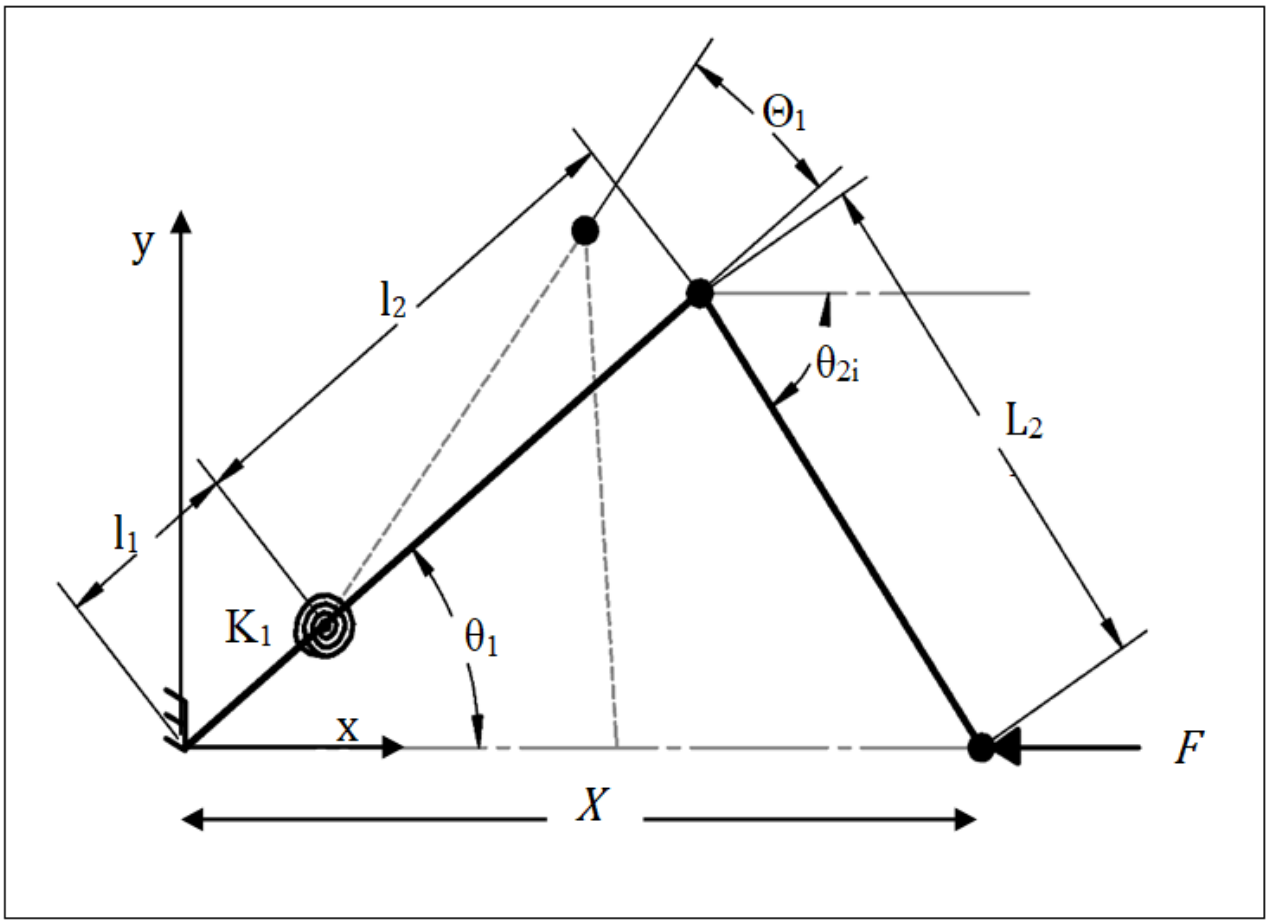

Figure 2: Internal forces analysis. Where E is the material modulus of elasticity, t is the link' thickness, and w is the link's width. The characteristic stiffness K_2 is calculated when link 2 buckles but, in this case, it will be used to the non-dimensional form later in this section. The close loop equations for the mechanism are:

$$l_1 cos(\theta_1) + l_2 cos(\theta_1 + \Theta_1) + l_2 cos(\theta_2) - X = 0 \tag{5}$$
$$l_1 sin(\theta_1) + l_2 sin(\theta_1 + \Theta_1) + l_2 sin(\theta_2) = 0 \tag{6}$$

Where θ_1, θ_2 are the link 1 and link 2 angles respectively and Θ_1 is the PRBM link 1 deflection angle. The virtual work equations were derived based on the defined independent variable (X, and θ_2) and the dependent variables(Θ_1 and F) are from Eq. (7) to (9).

$$\partial w = -Fdx - \frac{\partial v}{\partial x}dx = 0, where\ v = \frac{1}{2}K_1\Theta_1^2 \tag{7}$$

$$\frac{\partial v}{\partial x} = K_1\Theta_1\frac{\partial \Theta_1}{\partial x} \tag{8}$$

$$\frac{\partial \Theta_1}{\partial x} = -\frac{cos(\theta_2)}{l_2 sin(\Theta_1 + \theta_1 + \theta_2)} \tag{9}$$

To better control the design concept, the equations are derived to be non-dimensional using these conditions:

$$m = \frac{sin(\theta_1)}{sin(\theta_{2i})} = \frac{L_2}{L_1} \tag{10}$$

$$\nu = \frac{K_1}{K_2} \tag{11}$$

$$\xi = \frac{F}{K_1} = F\frac{L_1^2}{K_\Theta \gamma E I_1} \tag{12}$$

Eq. (10) to (12) are used to form the non-dimensional governing Eq. (13) which will be solved numerically with Eq. (5) and (6):

$$\xi + L_1\Theta_1\frac{\partial \Theta_1}{\partial x} = 0 \tag{13}$$

The solution of the the governing Eq. (13) depends on variable input parameters as in table 2 and constant input parameters (Θ, K_Θ, E). The numerical solutions will generate the values (ν, Θ_1, ξ) for each sets of input values as in Table 2. The design outputs are obtain using the numerical solutions as the following (refer Eq. (14) to (19)):

$$L_1 = (X - \frac{\Delta}{2})\frac{1}{cos(\theta_1)} \tag{14}$$

$$L_2 = L_1\sqrt{(\frac{\Delta}{2L_1})^2 + sin(\theta_1)^2} \tag{15}$$

The initial angle of link 2 (θ_{2i}) can be calculated as:

$$\theta_{2i} = cos^{-1}(\frac{\Delta}{2L_2}) \tag{16}$$

$$w_1 = \frac{\partial y}{E}\frac{1}{\gamma K_\Theta}\frac{L_1}{\Theta_1} \tag{17}$$

$$w_2 = \sqrt[3]{\frac{m}{2\nu}}w_1 \tag{18}$$

$$F_{max} = \frac{\gamma K_\Theta E I_1 \xi}{L_1^2} \tag{19}$$

Where ∂y is the yield stress of the material which in this study Polypropylene material is selected with 1.35 GPa young's modulus E and 35 MPa yield stress ∂y. The design outputs are presented in table 3 for different sets of variable input parameters. The maximum linear deflection Δ and the maximum horizontal footmark X should constrain to satisfy the condition $\Delta \leq X$ which ensure the mechanism follow the geometric rules of bi-stability. Th design concept relay on Theta-cap Θ_1 and F_{max} because they control the amount of force required to deform the mechanism between its bi-stable configurations. Therefore, these two outputs are optimized in the following section,

2.2. Response surface methodology:

Following step by step procedure is adopted to derive mathematical models based on quadratic level regression with surface plots for outputs for achieving optimum condition.

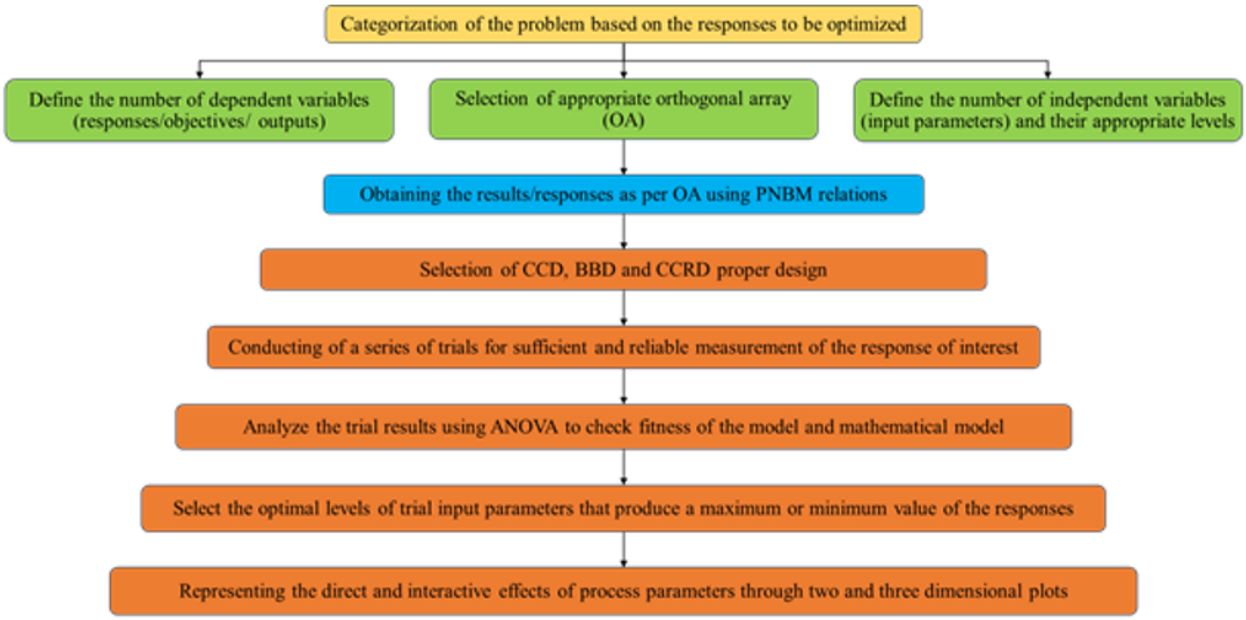

Figure 3: Various steps involved in RSM process The maximum applied force on the compliant link (F_{max}) and the PRBM angle of link1 (Theta-cap-Θ_1) are measured as output/objective characteristics. The Fmax and Theta-cap (Θ_1) were measured by Kinematic and virtual work relationships. In analysis, Box-benhen design (BBD) has been used as a module of response surface methodology. Table 3 shows the design of trials and obtained the value of Fmax and Theta-cap (Θ_1) using the various levels of input factors as provided in Table 2.

Table 2: 3Various levels of input parameters of bi-stable compliant mechanism

Input variables	Units	Values
Maximum horizontal footprint (X)	mm	30, 40, 60
Mechanism's maximum linear deflection (Δ)	mm	20, 30, 40, 50
Initial angle of link 1 (θ_1)	deg	20, 30, 40, 50, 60, 70
Material thickness (t)	mm	3, 6, 12

Table 3: Experimental runs as per L27 Orthogonal Array

N0.	X	Δ	θ_1	t	Theta-Cap ($Theta_1$) in radians	F_{max} in N
1	30	20	20	3	10	0.390126
2	30	30	30	6	22.5	0.404902
3	30	20	40	12	5.5	1.748708
4	30	30	50	6	15	0.528984
5	30	20	60	12	2.5	3.808687
6	30	30	70	3	6.75	0.536966
7	40	20	30	12	3	2.938802
8	40	30	40	3	9	0.326534
9	40	40	50	6	15	0.528984
10	40	20	60	6	1.8	1.020417
11	40	30	70	12	1.5	5.877603
12	40	40	20	3	29.5	0.16526
13	40	20	40	12	2.2	4.098535
14	40	30	50	3	6.5	0.391261
15	40	40	60	6	12	0.633679
16	60	20	70	3	0.001	330.6152
17	60	30	20	6	5	1.190215
18	60	40	30	12	7	1.88923
19	60	50	50	12	8.5	1.281277
20	60	20	60	3	0.6	1.836751
21	60	30	70	6	0.1	16.53076
22	60	40	20	3	10	0.390126
23	60	50	30	6	12	0.665822
24	60	20	40	12	0.5	26.44921
25	60	30	60	6	1.8	1.020417
26	60	40	70	12	2.75	2.09845
27	60	50	20	3	15	0.301227

3. Results and Discussions

3.1. Stochastic assessment and attainment of mathematical model (MM)s

The stochastic examination and competency of generated MMs are verified by means of Analysis of Variance (ANOVA) at 95% assurance rank. The response surface model corresponding to Fmax and Theta-cap (Θ_1) on the findings of direct and quadratic order by means of ANOVA are described in Table 4 and 5. Evaluation of influence of input factors, data examination and higher order (quadratic) model development is done by Stochastic Minitab V20 software. Then the proficiency of model is authenticated via R2 value (co-efficient of determination) to prove the adequacy of regression model. In this work, R^2 was seen as 85.3% for Fmax and 86.7 % for Theta-cap (Θ_1) which are nearer to one means it shows logical conformity and designates competence of established MMs. The satisfactory accuracy percentage for F_{max} and Theta-cap (Θ_1) is exceeding minimum value identifies acceptable MM difference.

Table 4: Analysis of Variance for Theta cap (Θ_1)

Source	**DF**	**Adj SS**	**Adj MS**	**F-Value**	**P-Value**
Model	14	1325.41	94.672	46.02	0.000
Linear	4	855.51	213.876	103.97	0.000
X	1	339.25	339.248	164.92	0.000
Δ	1	279.32	279.324	135.79	0.000
θ_1	1	247.78	247.783	120.45	0.000
t	1	2.12	2.120	1.03	0.330
Square	4	29.75	7.438	3.62	0.037
$X * X$	1	20.54	20.543	9.99	0.008
$\Delta * \Delta$	1	2.28	2.282	1.11	0.313
$\theta_1 * \theta_1$	1	0.06	0.057	0.03	0.871
$t * t$	1	4.94	4.937	2.40	0.147
2-Way Interaction	6	250.85	41.809	20.32	0.000
$X * \Delta$	1	102.65	102.651	49.90	0.000
$X * \theta_1$	1	75.60	75.604	36.75	0.000
$X * t$	1	3.22	3.217	1.56	0.235
$\Delta * \theta_1$	1	50.65	50.647	24.62	0.000
$\Delta * t$	1	0.10	0.102	0.05	0.828
$\theta_1 * t$	1	4.35	4.353	2.12	0.171
Error	12	24.68	2.057		
R^2		98.17%			
R^2 (adjusted)		96.04%			

Table 5: Analysis of Variance of F_{max}

Source	**DF**	**Adj SS**	**Adj MS**	**F-Value**	**P-Value**
Model	14	61220	4372.9	1.22	0.369
Linear	4	3383	845.8	0.24	0.913
X	1	2631	2630.9	0.73	0.408
Δ	1	1623	1622.8	0.45	0.514
θ_1	1	1054	1054.1	0.29	0.597
t	1	1919	1918.6	0.54	0.478
Square	4	11458	2864.5	0.80	0.548
$X * X$	1	190	190.0	0.05	0.822
$\Delta * \Delta$	1	3432	3431.7	0.96	0.347
$\theta_1 * \theta_1$	1	6291	6290.7	1.76	0.210
$t * t$	1	1081	1080.5	0.30	0.593
2-Way Interaction	6	22920	3819.9	1.07	0.433
$X * \Delta$	1	5287	5287.3	1.48	0.248
$X * \theta_1$	1	3545	3545.4	0.99	0.340
$X * t$	1	1911	1911.3	0.53	0.479
$\Delta * \theta_1$	1	2926	2925.9	0.82	0.384
$\Delta * t$	1	2850	2849.7	0.80	0.390
$\theta_1 * t$	1	4967	4966.6	1.39	0.262
Error	12	43000	3583.3		

Total	26	104221			
R^2		85.74%			
R^2 (adjusted)		89.61%			

From the ANOVA examination after eliminating the irrelevant terms, the second order (quadratic) MMs (i.e., in form of tangible values) for F_{max} and Theta-cap (Θ_1) are found and shown in Eq. (20) and (21).

$$\begin{aligned} Theta-cap(\Theta_1) =& 7.53 - 1.097 * X + 2.387 * \Delta - 0.300 * \theta_1 + 0.038 * t + 0.01162 * X * X \\ &+ 0.00466 * \Delta * \Delta + 0.00025 * \theta_1 * \theta_1 - 0.0584 * t * t - 0.03097 * X * \Delta \\ &+ 0.00976 * X * \theta_1 + 0.01127 * X * t - 0.01438 * \Delta * 1 + 0.0024 * \Delta * t \\ &+ 0.00846 * \theta_1 * t \end{aligned} \tag{20}$$

$$\begin{aligned} F_{max} =& 23 + 1.9 * X + 0.9 * \Delta - 5.01 * 1 + 2.0 * t + 0.035 * X * X \\ &+ 0.181 * \Delta * \Delta + 0.0821 * \theta_1 * \theta_1 + 0.86 * t * t - 0.222 * X * \Delta \\ &+ 0.0669 * X * \theta_1 - 0.275 * X * t - 0.109 * \Delta * 1 + 0.408 * \Delta * T \\ &- 0.286 * \theta_1 * t \end{aligned} \tag{21}$$

The pareto plot of responses against each factor shows that, most influential factors are X, Δ and θ_1 as individually and $Xx\Delta$, $Xx\theta_1$ and $\Delta x\theta_1$ as at interaction level between factors and X^2 as at square level of factors on Theta-cap (Θ_1) observed. Whereas in case of F_{max} only θ_1^2 square $\theta_1 xt$ and $Xx\Delta$ as at interaction level showing some influence.

Where X, Δ, θ_1, and t are the maximum horizontal footprint, the mechanism's maximum linear deflection, the initial angle of link 1, and the material thickness, respectively. Generally, stochastic analysis imitated the investigational results are well-fitting in forecasted ones and the accurateness of the MM is enough to extend work with optimized inspections on governing bi-compliant CM input parameters.

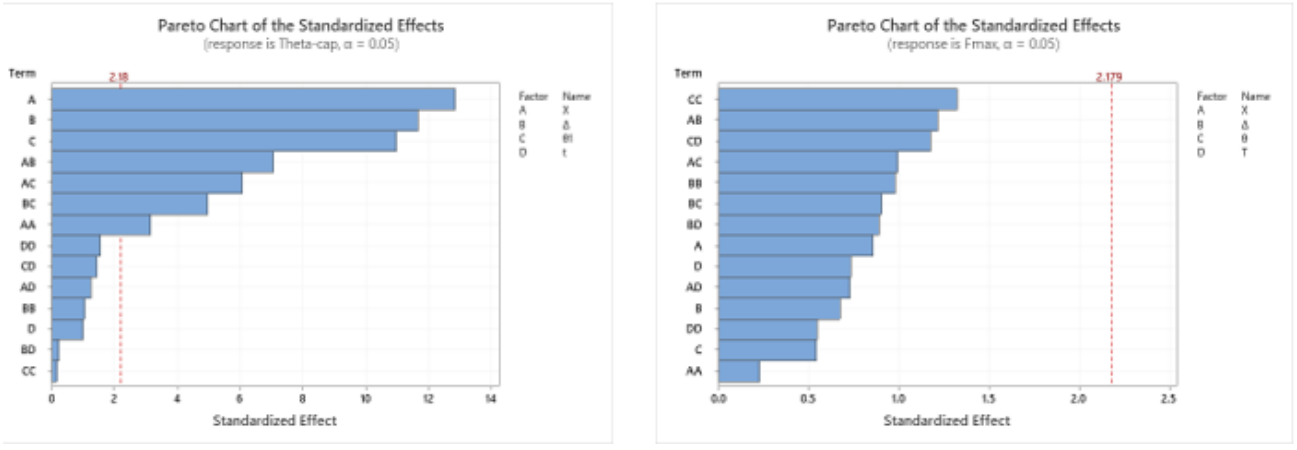

Figure 4: Pareto plot for responses (a) Theta-cap (Θ_1) (b) F_{max}

3.2. Influence of input factors on F_{max}

The influence of maximum horizontal footprint in combination (X) with Δ, θ_1, and t on F_{max} is shown in Figure 5a to 5c. From the response plots of F_{max}, it is observed that the F_{max} is minimum at lower value of X for intermediate value of Δ, at higher value of X for mid value of θ_1, and mid value of t. It is reliable with the statement that the less linear movement of the slider, the less force is required. Hence, F_{max} of the CM also shown minimum at lower value of Δ for intermediate value of θ_1, and at mid value of Δ and for lower value of t as shown in responses plot of F_{max} with interaction effect are seen in Figure 5d to 5e. This is due to fact that the actuating force is minimized as distance between the stable configurations are close to each other resulted in better stability of system to be operated with minimum load. The interaction influence of θ_1 and thickness t on F_{max} is shown in Figure 5f. It is observed that mid value of θ_1 and t causes F_{max} to decrease. It can be justified with the fact that at minimum initial angle of link 1 θ_1, the link would require large force to bending the link as its moves to the second stable configuration which increases the stresses on the joints and the other link. Fig. 5c and 5e demonstrate the effect of having long link with thicker cross-section to overcome the out-of-plane motion that would requires minimum force when Δ at mid value meaning the linear transition between the stable configurations is intermediate.

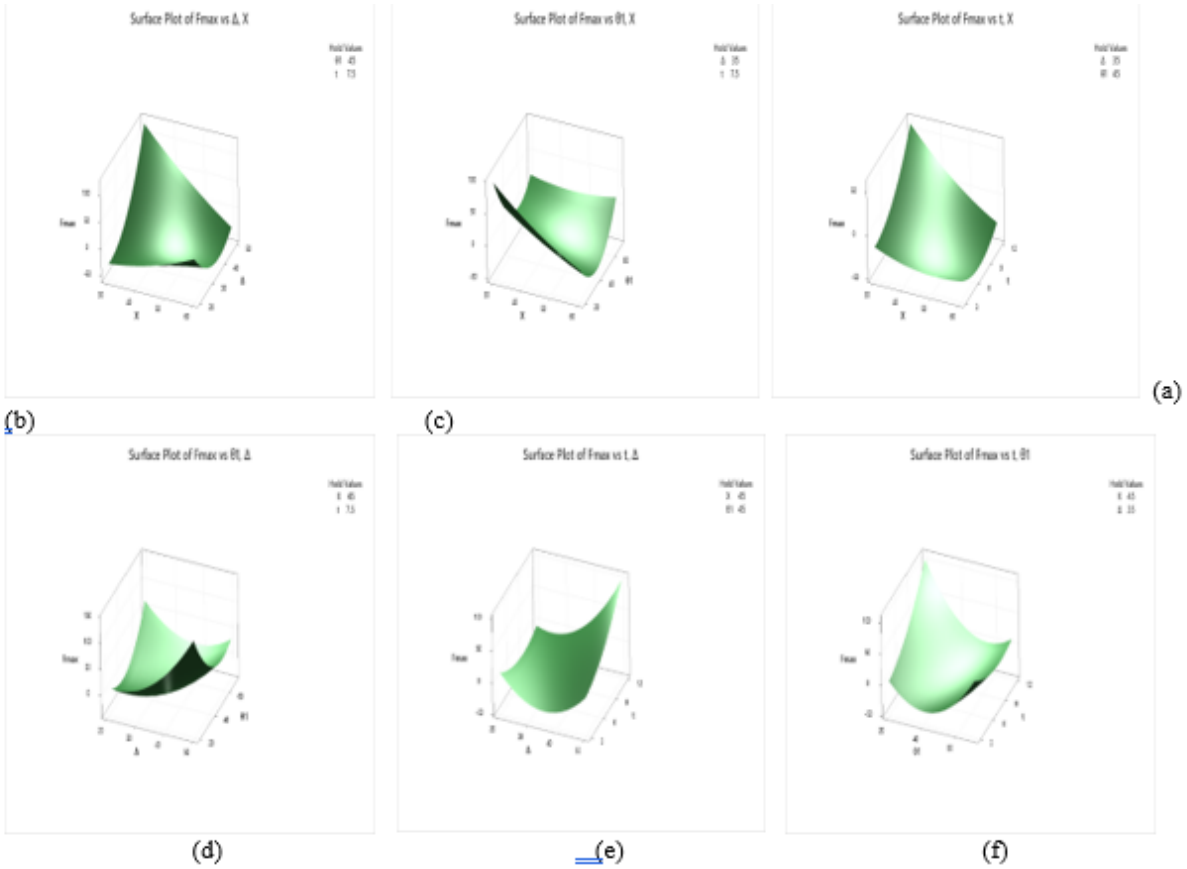

Figure 5: 3D Surface plots of F_max for the (a) effect of X and Δ, (b) effect of X and θ_1 (C) effect of X and t, (d) effect of Δ and θ_1, (e) effect of Δ and t and (f) effect of θ_1 and t.

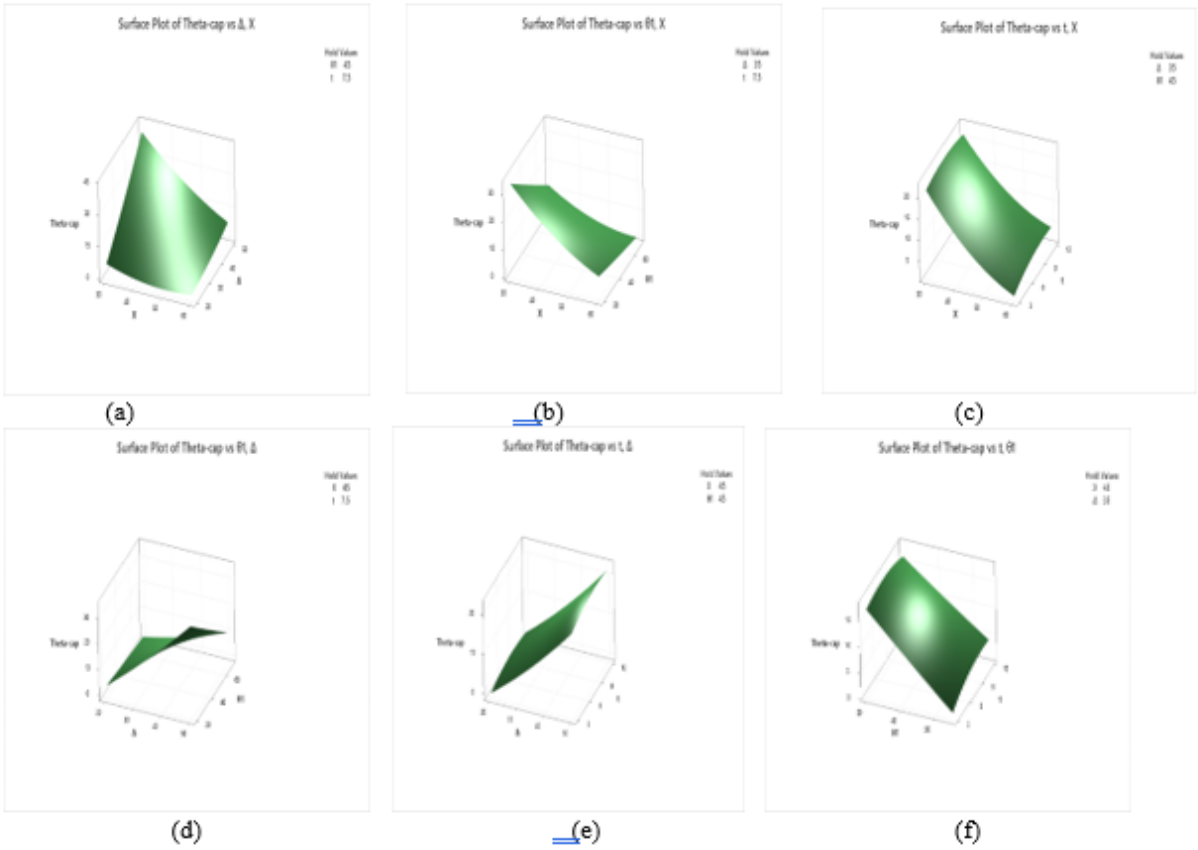

Figure 6: 3D Surface plots of F_max for the (a) effect of X and Δ, (b) effect of X and θ_1 (C) effect of X and t, (d) effect of Δ and θ_1, (e) effect of Δ and t and (f) effect of θ_1 and t.

3.3. Influence of input factors on Theta-cap.

The 3D response plots are depicted in Figure 6 (a-f) illustrate the impact of input factors on Theta-cap (Θ_1). It is noticed that the impact of input parameters on estimating Theta-cap (Θ_1) have shown different trend like in the case of Fmax of the CM. Figure (6a-6c) depicts the impact of $X\&\Delta$, $X\&\ \theta_1$ and $X\&t$ on Theta-cap (Θ_1) which show that, Theta-cap (Θ_1) increases 3 to 35 radians at low value of $X = 30$ for higher values of $\Delta = 50$, $t = 12$ and $\theta_1 = 600$. Figure (4d-4e) reflect the impact of $\Delta\&\theta_1$ and $\Delta\&t$ on Theta-cap (Θ_1) show that, it has increased from 2 to 20 radians at highest values of Δ, θ_1, and t. this is due to fact that long distance between the stable configurations would require the compliant link to deflect more to accommodate the bi-stable behavior. Finally, referring figure 4f showing the impact of 1 and t on Theta-cap (Θ_1) in a way that theta-cap attaining maximum value at lowest value of θ_1 irrespective t value. Due to fact it can be authenticated that at maximum Theta-cap (Θ_1), which is large deflection of link 1, the link' stiffness is lower and less stresses will be exerted. Fig. 6b, 6d, and 6f show that low initial angle θ_1 would lead to large deflection in the link at long linear transition of the stable configurations. However, the reducing the footprint of the mechanism X makes the ink bend more which increasing Theta-cap (Θ_1). On the other hand, the force required can be minimized while allowing Theta-cap (Θ_1) to maximized when the value of the footprint of the mechanism and the mechanism' linear displacement of slider are close at mid value of θ_1 and low thickness t.

3.4. Multi-response optimization of Bi-compliant CM input parameters.

especially when one factor has to be minimized and other output to be maximized. Desirability approach can handle this complex analysis mechanism process. It has great impact in selecting optimal input factors with all constraints defined. To optimize simultaneously multi-outputs, the factors undergo desirability approach [27]considered as an exclusive optimization approach in various engineering problems. In a multiple-target zone, all objectives/outputs must satisfy combined goals of a process with an assessing procedure for solution guarantying how it has been achieved. Using an established composite desirability of RS optimization technique, both outputs (refer Table 5) i.e., Fmax and Theta-cap (Θ_1) are enhanced all together by means of resulted statistical models as expressed in Eq. (20) and (21). The plots of desirability approach as illustrated in Figure 7 portrays the optimal data set attained through stochastic RSM. It brings to light that, optimal set predicted maximum Theta-cap (Θ_1) of 29.5 radians and minimum Fmax of 8.55 N could be achieved for CM mechanism under input factor conditions like $X = 30$ mm, $\Delta = 38.06$ mm, $\theta_1 = 35.9581$ degrees and $t = 3$ mm (refer Table 6). Confirmation of these factors were checked at optimum set and obtained at both 95% PI and CI level as listed in Table 7.

Table 6: Parameters feasible bound values

Response	**Goal**	**Lower**	**Target**	**Upper**	**Weight**	**Importance**
Fmax	Minimum		0.2	330.615	1	0.9
Theta-cap (Θ_1)	Maximum	0.475789	29.5000		1	1

Table 7: Optimized set for the combination of factors

Solution	X	Δ	θ_1	t	F_{max} Fit	Theta-cap Fit	Composite Desirability
1	30	38.0654	35.9581	3	8.55007	29.5000	0.987232

Table 8: Confirmation of results at optimum set of parameters

Response	**Fit**	**SE Fit**	**95% CI**	**95% PI**
Fmax	8.6	61.1	(-124.6, 141.7)	(-177.8, 194.9)
Theta-cap	29.50	1.46	(26.31, 32.69)	(25.03, 33.97)

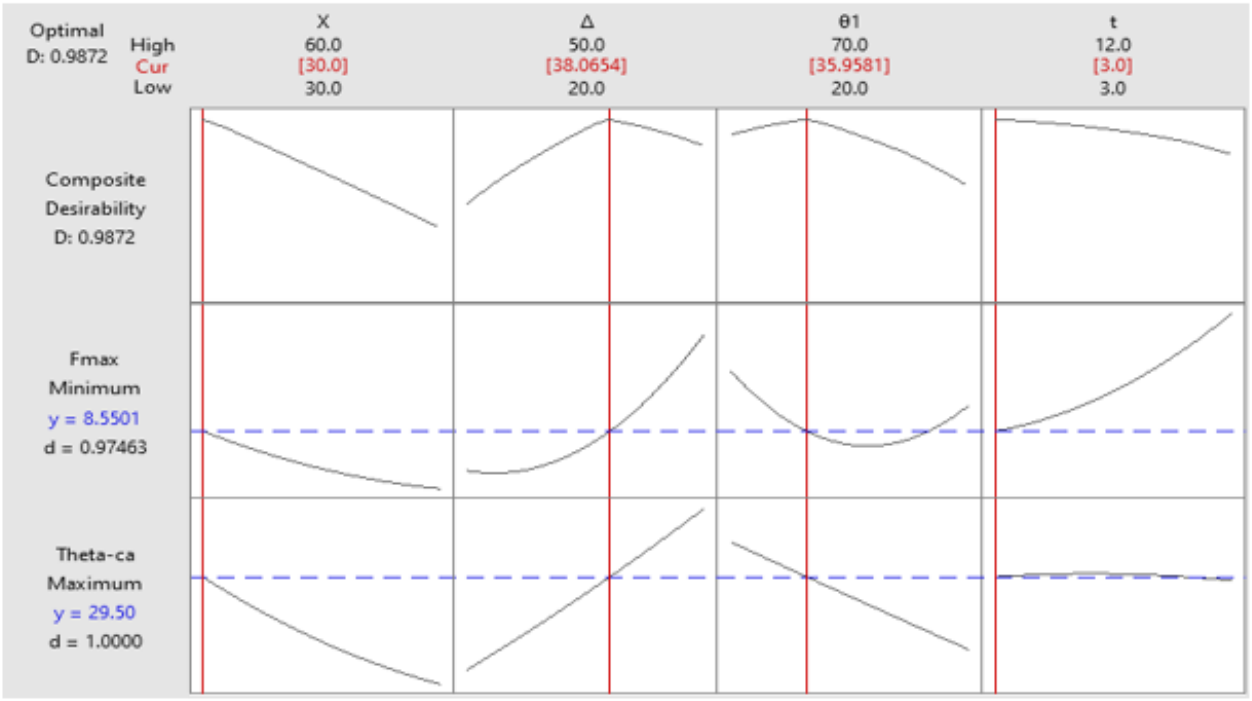

Figure 7: Desirability approach results of statistical optimization

4. Conclusions

Bi-compatible compliance mechanism of fixed-pinned beam have been generated through Pseudo-Rigid-body model. The output results of mechanisms like Fmax and Theta-cap (Θ_1) are examined by means of Box-Behnken design of RS technique. Relationship templates are generated to forecast the outputs of mechanism of the CM. The ensuing conclusions are comprehended from the current investigations.

- Mathematical models of Fmax and Theta-cap (Θ_1) were extracted to link up the governing input elements like the maximum horizontal footprint, the mechanism's maximum linear deflection, the initial angle of link 1, and the material thickness.
- The maximum Theta-cap (Θ_1) of 29.5 radians and minimum of Fmax of 8.5501 N could be achieved by considering optimal CM input factors having X of 30 mm,Δ = 38.06 mm, 1=35.9581 degrees and t=3 mm.
- Impact of 1followed by t has predominant effect on Fmax and Theta-cap (Θ_1). However, X has insignificant effect on outputs.
- The higher θ_1 offered higher Theta-cap (Θ_1) and minimum F_{max}. On contrary, F_{max} increased and Theta-cap (Θ_1) decreased with increase of thickness from 3 to 12 mm.

To obtain large number of optimal combination of factors for outputs, Genetic algorithm and Particle swarm optimization can be conducted and compared to meet the industrial requirements.

ACKNOWLEDGEMENT
The authors of would like to thank the Deanship of Scientific Research at Umm Al-Qura University for supporting this work by Grant Code 20-ENG-4-13-0002.

Conflict of Interest

The authors declare that there is no potential conflict of interest concerning research, authorship, and/or publication of this article.

References

[1] Howell, L.L., Compliant mechanisms. 2001, New York: Wiley. xvii, 459 p.
[2] Chen, T., J. Mueller, and K. Shea, Integrated design and simulation of tunable, multi-state structures fabricated monolithically with multi-material 3D printing. Scientific reports, 2017. 7: p. 45671.
[3] Alfattani, R. and C. Lusk, Shape-Morphing Using Bistable Triangles With Dwell-Enhanced Stability. Journal of Mechanisms and Robotics, 2020. 12(5).
[4] Alfattani, R., Design of Shape-morphing Structures Consisting of Bistable Compliant Mechanisms. 2019, University of South Florida: Ann Arbor. p. 125.
[5] Montalbano, P. and C. Lusk. Multistable Shape-Shifting Surfaces. in ASME 2012 International Design Engineering Technical Conferences and Computers and Information in Engineering Conference. 2012.
[6] Anilkumar, P.M., et al., Design optimization of multistable variable-stiffness laminates. Mechanics of Advanced Materials and Structures, 2019. 26(1): p. 48-55.
[7] Arrieta, A.F., et al., Dynamics and control of twisting bi-stable structures. Smart Materials and Structures, 2018. 27(2).
[8] Mukherjee, A., et al., Modeling and design of a class of hybrid bistable symmetric laminates with cantilever boundary configuration. Composite Structures, 2020. 239: p. 14.
[9] Zhang, S. and G. Chen. Design of Compliant Bistable Mechanism for Rear Trunk Lid of Cars. in Intelligent Robotics and Applications. 2011. Berlin, Heidelberg: Springer Berlin Heidelberg.
[10] Kota, S. and G.K. Ananthasuresh, Designing compliant mechanisms, in Mechanical Engineering-CIME. 1995. p. 93+.
[11] Salamon, B.A. Mechanical advantage aspects in compliant mechanisms design. in Advances in Design Automation, DA Hoeltzel, ed., 18th ASME Design Automation Conference. 1989.
[12] Hussein, Z., Leading to intention: The role of attitude in relation to technology acceptance model in e-learning. Procedia Computer Science, 2017. 105: p. 159-164.
[13] Chanthasopeephan, T., et al., Impact reduction mobile robot and the design of the compliant legs. Robotics and Autonomous Systems, 2014. 62(1): p. 38-45.
[14] Zhang, X. and W. Hou, Dynamic analysis of the precision compliant mechanisms considering thermal effect. Precision Engineering, 2010. 34(3): p. 592-606.
[15] Motsinger, R.N. and P. Stein, Flexural devices in measurement systems. Measurement Engineering, 1964. 1: p. 383-435.
[16] Miller, E., Plastics Products Design Handbook: Materials and components. Vol. 8. 1981: Marcel Dekker.
[17] Bisshopp, K. and D. Drucker, Large deflection of cantilever beams. Quarterly of Applied Mathematics, 1945. 3(3): p. 272-275.
[18] Chen, G., Y. Ma, and J. Li, A tensural displacement amplifier employing elliptic-arc flexure hinges. Sensors and Actuators A: Physical, 2016. 247: p. 307-315.
[19] NGUYEN, K.-V., H.-H. PHAM, and H.-T. PHAM. Multi-objective Optimization of a Linear Flexure-Based Mechanism Using Pseudo Rigid-Body Diagram Analysis and FEA-Based Response Surface Methodology. in The 3rd ASEAN Smart Grid Congress The 5th International Conference on Sustainable Energy. 2017.
[20] Du, Y., L. Chen, and Z. Luo, Topology synthesis of geometrically nonlinear compliant mechanisms using meshless methods. Acta Mechanica Solida Sinica, 2008. 21(1): p. 51-61.
[21] Su, H.-J. and J.M. McCarthy, Synthesis of bistable compliant four-bar mechanisms using polynomial homotopy. 2007.
[22] Limaye, P., et al., A compliant mechanism kit with flexible beams and connectors along with analysis and optimal synthesis procedures. Mechanism and machine theory, 2012. 49: p. 21-39.
[23] Seryasat, O. R., Zadeh, H. G., Ghane, M., Abooalizadeh, Z., Taherkhani, A., & Maleki, F. (2013). Fault Diagnosis of Ball-bearings Using Principal Component Analysis and Support-Vector Machine. Life Science Journal, 10(1s), 393-397.
[24] Ghane, Mahdi, Amir R. Nejad, Mogens Blanke, Zhen Gao, and Torgeir Moan. "Statistical fault diagnosis of wind turbine drivetrain applied to a 5MW floating wind turbine." In Journal of Physics: Conference Series, vol. 753, no. 5, p. 052017. IOP Publishing, 2016.
[25] Ghane, Mahdi, and Mohammad Jafar Tarokh. "Multi-objective design of fuzzy logic controller in supply chain." Journal of Industrial Engineering International 8.1 (2012): 10.

[26] Gallego, J.A. and J. Herder. Synthesis methods in compliant mechanisms: An overview. in International Design Engineering Technical Conferences and Computers and Information in Engineering Conference. 2009.
[27] Huy-Tuan, P., V. Nguyen, and V. Mai, Shape optimization and fabrication of a parametric curved segment prosthetic foot for amputee. Journal of Science and Technology: Technical Universities, 2014. 102: p. 89-95.
[28] Dao, T.-P., S.-C. Huang, and N. Le Chau, Robust parameter design for a compliant microgripper based on hybrid Taguchi-differential evolution algorithm. Microsystem Technologies, 2018. 24(3): p. 1461-1477.
[29] Nguyen, V.-K., H.-T. Pham, and H.-H. Pham. Optimal design of high precision compliant guide mechanism using gene algorithm and Taguchi-based sensitivity analysis. in 2017 International Conference on System Science and Engineering (ICSSE). 2017. IEEE.
[30] Huang, S.-C. and T.-P. Dao, Design and computational optimization of a flexure-based XY positioning platform using FEA-based response surface methodology. International Journal of Precision Engineering and Manufacturing, 2016. 17(8): p. 1035-1048.
[31] Howell, L.L., A. Midha, and T. Norton, Evaluation of equivalent spring stiffness for use in a pseudo-rigid-body model of large-deflection compliant mechanisms. 1996.